Varendra International Journal for Interdisciplinary Research 2026: 2(1), 115 - 128

ISSN: 3078-7017 (Online), 3078-7009 (Print)

https://doi.org/10.64296/vijir.v2i1.11

Received: April 10, 2026; Accepted: May 8, 2026

Enhanced Reverse Intersystem Crossing: Quantum Insights into Boron Containing Emitters for Organic Light Emitting Diode Application

Taherin Hoq

Department of Physics, Shahjalal University of Science and Technology, Sylhet – 3114, Bangladesh.

Nazia Chawdhury

Department of Physics, Shahjalal University of Science and Technology, Sylhet – 3114, Bangladesh. e-mail: nc-phy@sust.edu (Corresponding Author)

ABSTRACT

Thermally activated delayed fluorescence materials have emerged as promising candidates for next-generation organic light-emitting diodes due to their ability to harvest both singlet and triplet excitons without requiring heavy metals. In this work, a series of boron-based emitters are investigated to explore the effect of donor substitution on their electronic and excited-state properties. The parent molecule, a boron-oxygen fused molecule, 5,9-dioxa-13b-boranaphtho[3,2,1-de]anthracene, was systematically modified with various donor moieties like acridine and carbazole derivatives to form TBA-Ac, TBA-3Cz, TBA-P3Cz, BBAC-Ac and BBAPCAc. The structural optimization, frontier molecular orbital analysis and excited-state characterization of these emitters collectively revealed that donor incorporation strongly influences the singlet-triplet energy separation and spin-orbit interaction, which are critical for efficient reverse intersystem crossing. The parent compound exhibited a large singlet-triplet gap, prohibiting reverse intersystem crossing and eliminating thermally activated delayed fluorescence behaviour. In contrast, the donor-substituted derivatives showed significantly reduced singlet-triplet gap values enabling effective thermal upconversion. TBA-Ac demonstrated the smallest singlet-triplet gap of 0.12 eV and the highest spin-orbit coupling matrix element, 1.54 cm^{-1}, resulting in the fastest reverse intersystem crossing rate, k_{RISC}, of 1.26×10^6 s^{-1}, establishing it as the most efficient thermally activated delayed fluorescence candidate. BBAPC-Ac also showed strong spin-orbit coupling and high k_{RISC}, confirming that acridine-carbazole donor combinations effectively promote singlet-triplet conversion. The results demonstrate that strategic donor engineering around the boron–oxygen core can effectively accelerate the reverse intersystem crossing process. This work establishes a clear structure-property relationship, offering a rational design strategy for developing high-performance, metal-free thermally activated delayed fluorescence emitters.

Keywords: Reverse Intersystem Crossing; Boron Containing Emitters; Thermally Activated Delayed Fluorescence Organic Light Emitting Diode; Spin-Orbit Coupling Matrix Element.

1. Introduction

The 21st century has been defined by a revolution in visual technology, which has driven the growing demand for high-fidelity displays and energy-efficient lighting systems. This technological progress has been closely tied to the transformation of lighting systems from inefficient, heat generating bulbs to solid-state lighting devices that convert electrical energy directly into light with minimal loss. At the forefront of this revolution stand light-emitting diodes, which are celebrated for their remarkable energy efficiency, long lifespan, and design flexibility (Baldo, et al., 1998). Among solid-state lighting devices, organic light-emitting diodes (OLEDs) have emerged as a revolutionary class of materials that combine efficiency with versatility. OLEDs are self-emissive that allows wide viewing angles, fast response times and presents the potential for transparent, rollable, and flexible display panels. Structurally, an OLED is a complex multilayered solid-state device consisting of a thin organic film sandwiched between two electrodes, a reflective metal cathode and a transparent anode, often made of indium tin oxide. When an external voltage is applied, electrons are injected from the cathode and holes from the anode. These charges migrate through their respective transport layers and recombine within the emissive layer to form excitons, which subsequently decay radiatively to emit light, a process known as electroluminescence.

OLED technology is currently subject to huge achievements in the premium display market. Despite these achievements, significant challenges remain particularly in materials science and device longevity. While red and green phosphorescent or thermally activated delayed fluorescence (TADF) materials have achieved impressive efficiencies, developing a stable, high-efficiency deep-blue emitter remains a critical objective for researchers (Hiroki Uoyama, 2012; J. H. Burroughes, 1990). The scarcity and cost of heavy metals like iridium and platinum, which are often used in phosphorescent OLEDs, further motivate the search for sustainable alternatives. Boron-based TADF materials, for instance, represent a promising direction due to their metal-free composition and potential for high efficiency (Gloria Hong, 2021).

A fundamental limitation in OLEDs arises from the quantum spin statistics which distates the ratio of singlet to triplet excitons is statistically fixed at 1:3. In conventional fluorescent organic materials, only the singlet excitons undergo radiative decay to emit light, restricting the internal quantum efficiency (IQE) to a theoretical maximum of 25%, while the non-emissive triplet excitons dissipate energy through non-radiative thermal processes. This intrinsic inefficiency has driven the development of successive generations of emitter materials designed to harness triplet excitons and thereby enhance overall device performance (Reineke, 2014) (H. Yersin, 2011). The conventional first-generation fluorescent emitters only utilize singlet excitons, capping IQE at 25%. While second-generation phosphorescent emitters achieve 100% IQE by using heavy metals like iridium to enable spin-orbit coupling (SOC), their high cost and environmental toxicity have led to the development of third-generation TADF OLEDs. These materials, emerged as a

sustainable alternative that can achieve near-unity exciton utilization without relying on heavy metals. The principle behind TADF lies in the conversion of non-emissive triplet excitons into emissive singlets through a thermally driven process known as reverse intersystem crossing (RISC). (Figure 1.1) For this mechanism to be efficient, the energy gap between the lowest singlet excited state (S_1) and the lowest triplet excited state (T_1) must be minimal, typically less than 0.2 eV. At room temperature, the available thermal energy is sufficient to bridge this small gap, enabling triplet excitons to convert back into singlets and subsequently decay radiatively. This delayed fluorescence effectively recycles the triplet population, allowing TADF materials to achieve internal quantum efficiencies approaching 100% without the environmental or economic drawbacks of metal-based systems (A. Endo, 2009) (Adachi, 2014) (Yuyu Pan, 2014) (Endo, et al., 2011).

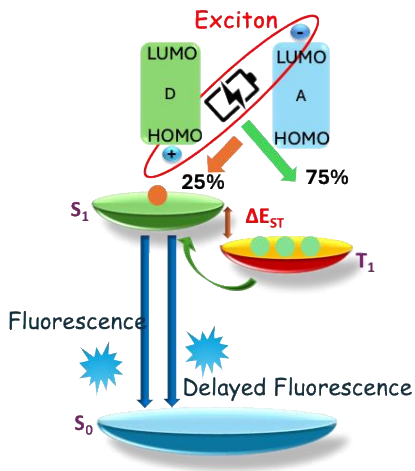

Figure 1.1. Schematic diagram of an OLED showing the process of light emission

The efficiency of TADF is inherently tied to molecular design, particularly the minimization of the singlet-triplet energy gap (ΔE_{ST}). The exchange energy, which dictates ΔE_{ST}, depends on the spatial overlap between the electron and hole wavefunctions in the excited state. Therefore, successful TADF emitters are typically constructed with donor-acceptor (D-A) molecular architectures that spatially separate the highest occupied molecular orbital (HOMO) and lowest unoccupied molecular orbital (LUMO). This separation reduces orbital overlap and consequently lowers the exchange energy, resulting in a small ΔE_{ST} which leads to efficient RISC. In such systems, the HOMO is localized on the donor moiety, while the LUMO is localized on the acceptor, promoting charge-transfer character in the excited state. This configuration not only facilitates exciton conversion but also enhances colour tunability and emission stability (Y. Olivier, 2018).

Experimental and theoretical studies have highlighted the potential of boron-based TADF materials for high-efficiency OLEDs. It has been demonstrated that a series of multi-resonance boron-nitrogen emitters exhibiting narrowband emission and minimal ΔE_{ST}, achieving high colour purity and efficient exciton utilization (Takuji Hatakeyama, 2016). Similarly, reports show that boron-oxygen fused TADF molecules with efficient blue

emission, underscores the versatility of boron incorporation in tuning photophysical properties (Numata, 2015) (Hyung Jong Kim, 2020). The unique electronic features of tricoordinate boron provides several advantages for TADF applications. The vacant p-orbital renders boron a strong Lewis acid, promoting efficient electron acceptance, while the inherent rigidity of boron-containing cyclic structures stabilizes the molecular conformation and suppresses non-radiative decay pathways (Takuji Hatakeyama, 2016). Incorporation of boron not only enhances electron deficiency but also improves thermal stability and structural rigidity, both of which are essential for the operational stability of OLED devices. Overall, boron-based TADF emitters represent a promising strategy for the development of highly efficient, metal-free OLEDs. The combination of strong electron-accepting capability, tunable frontier orbitals, structural rigidity and thermal stability makes boron an invaluable component in the rational design of next-generation organic emitters. (Dae Hyun Ahn, 2019)

This work presents a comprehensive computational study on such boron-based thermally activated delayed fluorescence emitters with various donor substitutions like acridine and carbazole, aiming to explain the electronic and excited-state properties that govern efficient triplet harvesting in OLEDs.

2. Materials and Methodology

This study utilized a computational chemistry framework to predict the photophysical properties of six boron-based emitters: the parent compound *BA* which is a boron-based core and derivatives *TBA-Ac*, *TBA-3Cz*, *TBA-P3Cz*, *BBAC-Ac* and *BBAPC-Ac*. The chemical structure of six boron-based TADF emitters investigated in this study are presented in Figure 2.1.

All initial geometry optimizations and subsequent excited state calculations of these materials were performed using the DFT and TD-DFT method as implemented in Gaussian 16W36 (H.Chermette, 1998). Molecular visualizations and frontier molecular orbital (FMO) analyses were conducted using GaussView 6.0 software (M. J. Frisch, 2016). The equilibrium structure of the ground state (S_0) for each molecule was optimized without imposing any symmetry constraints using *DFT/B3LYP/6-31G** in Gaussian 16. The Density Functional Theory (DFT) method was employed for the geometry optimization. The hybrid exchange-correlation functional B3LYP was chosen due to its proven reliability in predicting molecular geometries and excitation energies of organic TADF emitters. B3LYP offers an excellent balance between computational cost and accuracy for ground-state organic molecular properties and is widely used for systems. The 6-31G* basis set was applied throughout geometry optimizations and TD-DFT calculations. The energies of S_1 and T_1 excited states were calculated using Time-Dependent DFT (TD-DFT) by conducting single-point excited state calculations based on the optimized S_0 geometries.

The complementary calculations for Spin-Orbit Coupling Matrix Elements (*SOCME*s) were performed using the ORCA program package (version 5.0) (Frank Neese, 2012). The magnitude of Spin-Orbit Coupling is quantified by the *SOCME*, $\langle S_1|\hat{H}SOC|T_1\rangle$, where $\hat{H}SOC$ is the spin-orbit coupling Hamiltonian. The *SOCME* values between the S_1 state and the

lowest triplet states (T_1, T_2, etc.) were calculated using the ORCA package. These calculations were performed as single-point computations on the Gaussian-optimized S_0 geometries. The *B3LYP functional* and the *def2-SVP basis set* were used.

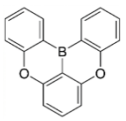	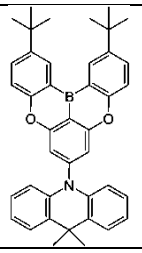
5,9-dioxa-13b-boranaphtho[3,2,1-*de*] anthracene ***BA***	10-(2,12-di-*tert*-butyl-5,9-dioxa-13b -boranaphtho[3,2,1-*de*]anthracen-7-yl)-9,9-dimethyl-9,10-dihydroacridine ***TBA-Ac***
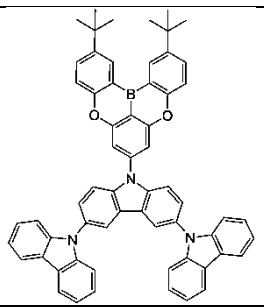	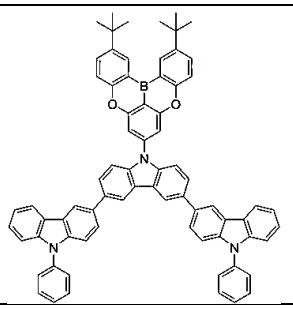
9′-(2,12-di-*tert*-butyl-5,9-dioxa-13*b*-boranaphtho[3,2,1-*de*] anthracen-7-yl)-9′*H*-9,3′:6′,9″-tercarbazole ***TBA-3Cz***	9′-(2,12-di-*tert*-butyl-5,9-dioxa-13*b*-boranaphtho[3,2,1-*de*]anthracen-7-yl)-9,9″-diphenyl-9*H*,9′*H*,9″*H*-3,3′:6′,3″-tercarbazole ***TBA- P3Cz***
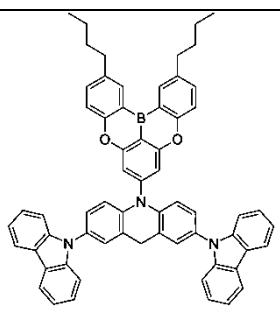	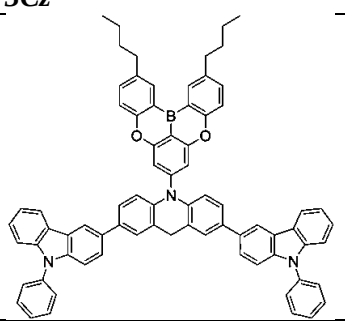
10-(2,12-dibutyl-5,9-dioxa-13b-boranaphtho[3,2,1-*de*] anthracen-7-yl)-2,7-bis(9H-carbazole-9-yl)-9,10-dihydroacridine ***BBAC-Ac***	10-(2,12-dibutyl-5,9-dioxa-13b-boranaphtho[3,2,1-*de*]anthracen-7-yl)-2,7-bis(9-phenyl-9H-carbazol-3-yl)-9,10-dihydroacridine ***BBAPC-Ac***

Figure 2.1. Investigated molecules and their chemical structures

The reverse intersystem crossing rate (k_{RISC}) was estimated using a simplified model based on Fermi's Golden Rule for a thermally activated process:

$$k_{RISC} \approx (2\pi / \hbar)\ |\langle S_1|\hat{H}_{SOC}|T_1\rangle|^2\ FCWD \qquad (1)$$

where, $\hbar$ is the reduced Planck's constant and $|\langle S_1|\hat{H}_{SOC}|T_1\rangle|^2$ is the square of the SOCME between S_1 and T_1. *FCWD* is the Franck-Condon Weighted Density of States, which for a small ΔE_{st} system can be approximated by the Boltzmann factor, $exp\ (-\Delta E_{st} / k_B T)$, where k_B is the Boltzmann constant, and T is the temperature.

The reorganization energies (λ) were calculated following the four-point method (Yuzhi Song, 2022). Based on the Marcus equation, the energy is set as

$$\lambda_{RISC} = E(S_1@T_1) - E\ (S_1) \qquad (2)$$

Here, $E(S_1@T_1)$ is the energy of the S_1 at the geometry of T_1 and $E(S_1)$ is the energy of the lowest singlet state.

3. Results and Discussions

The ground-state (S_0) geometries of the molecules *TBA-Ac*, *TBA-3Cz*, *TB-P3Cz*, *BBAC-Ac* and *BBAPC-Ac* along with the parent compound *BA* (Boron Acceptor) were fully optimized at the DFT/B3LYP/6-31G* level of the theory. Analysis of the frontier molecular orbitals (FMOs) confirms the strong charge-transfer (CT) character across all derivative molecules. For all five derivative compounds (*TBA-Ac*, *TBA-3Cz*, *TB-P3Cz*, *BBAC-Ac* and *BBAPC-Ac*), the Highest Occupied Molecular Orbital (HOMO) density is found to be predominantly localized on the electron-donating unit (D) of the molecule. Conversely, the Lowest Unoccupied Molecular Orbital (LUMO) density is concentrated almost entirely on the boron-containing electron-accepting unit (A). The optimized structures, HOMO and LUMO for all molecules are presented in Figure 3.1.

The FMO analysis reveals a stark contrast between the mother compound and its derivatives. In the unsubstituted *BA* molecule, both the HOMO and LUMO are delocalized over the entire π-conjugated core, including the boron atom. This significant spatial overlap indicates its large ΔE_{ST}. On the other hand, a consistent and clear pattern emerges across all five donor-acceptor derivatives. The HOMO and LUMO show a clean separation localizing on the Donor and Acceptor part of these molecules. This clean spatial separation observed in the optimized geometries, disrupts conjugation and confine the HOMO and LUMO to their respective molecular fragments. Thus, the spatial overlap between the HOMO and the LUMO is visually confirmed, directly supporting the molecular design principle aimed at minimizing the singlet-triplet energy gap. Figure 3.2 visually shows the energy level diagram of HOMOs and LUMOs of the materials.

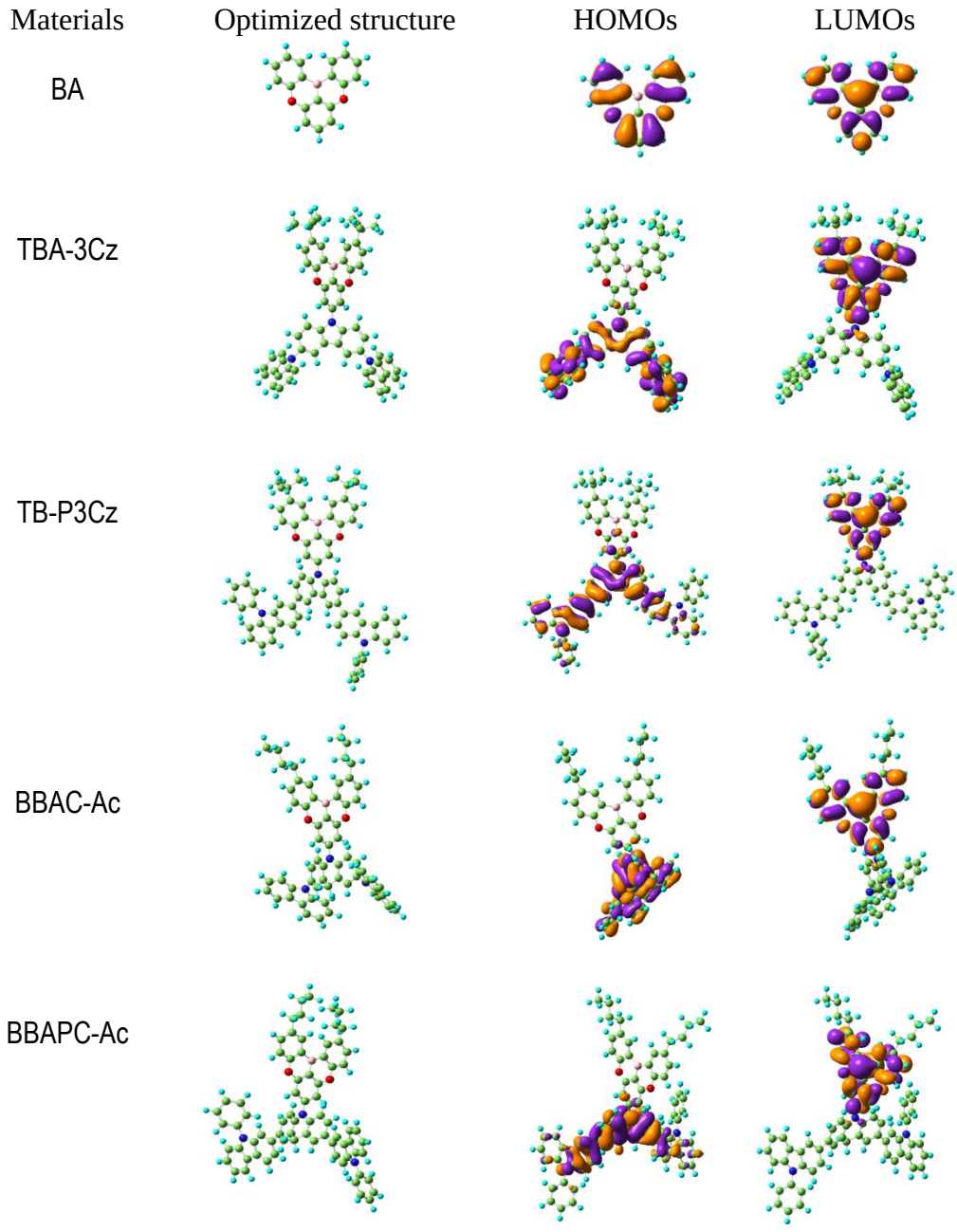

Figure 3.1. Optimized structures, HOMOs AND LUMOs of the materials

Figure 3.2 shows the energy levels of HOMOs and LUMOs of the materials. The observed trend reflects a systematic enhancement of donor strength from BA to BBAPC-Ac. The

gradual narrowing of the HOMO-LUMO energy gap across the series highlights the effectiveness of molecular engineering in tuning the electronic properties of boron-based TADF emitters. These results confirm that strategic donor substitution not only modulates the electronic energy levels but also enhances charge-transfer characteristics, thus offering an effective pathway for designing materials with desired properties.

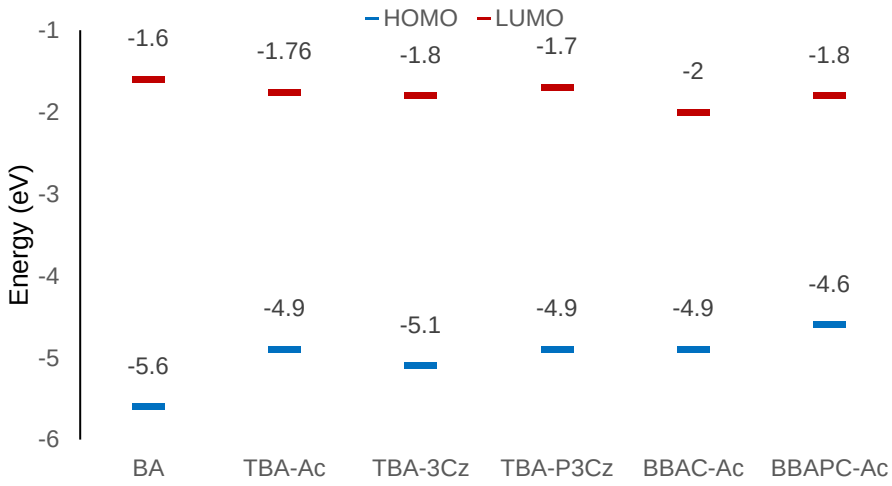

Figure 3.2. Calculated HOMO and LUMO energies of the molecules

The lower lying singlet and triplet levels are shown in Figure 3.3. TADF behaviour arises when the ΔE_{st} is small enough that room temperature provides the energy required to make RISC. Among all studied materials, *BA* exhibits the largest ΔE_{ST} value of 0.67 eV, indicating a wide energy gap between the singlet and triplet states. Such a large gap suggests that the molecule provide minimal TADF contribution, as the thermal energy available at room temperature is insufficient to promote efficient RISC. In contrast, dramatic reductions in ΔE_{ST} are seen across the series of substituted donor-acceptor derivatives, all falling well below the critical threshold necessary for efficient TADF. *TBA–Ac* shows a remarkably reduced ΔE_{ST} of 0.12 eV, signifying a highly favourable condition for TADF. The small ΔE_{ST} indicates enhanced charge transfer character, likely arising from the introduction of the acridine donor unit. This promotes efficient RISC within the material. The moderate ΔE_{ST} values observed for *TBA–3Cz* and *TB–P3Cz* are still sufficiently small to permit thermally assisted upconversion of triplet excitons that promote efficient RISC. The narrow ΔE_{ST} values of 0.19 eV and 0.17 eV are observed for *BBAC–Ac* and *BBAPC–Ac*, respectively. Incorporation of carbazole and acridine moieties contributes to effective charge transfer characters, thus presenting favourable ΔE_{ST}.

The gradual reduction in ΔE_{ST} across the substituted boron–acridine and boron–carbazole derivatives demonstrates the success of molecular engineering strategies in tuning excited-state energetics. The results clearly establish that introduction of strong electron-donating acridine and carbazole units onto the boron acceptor core significantly enhances charge-transfer character and reduces ΔE_{ST}, thus promoting favourable TADF behaviour.

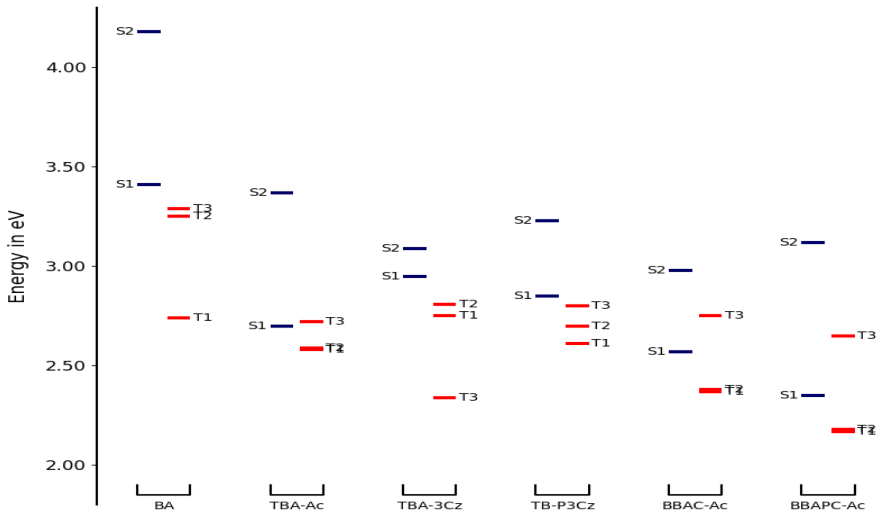

Figure 3.3. Energy levels with singlet and triplet states

The correlation between the HOMO–LUMO energy gap (E_{HL}) and the ΔE_{ST} reveals the electronic nature of the studied boron-based TADF materials. The reduction in ΔE_{st} is a direct result of the donor-acceptor architecture. The spatial separation of the HOMO and LUMO, as visualized in Figure 3.4 minimizes the wavefunction overlap integral.–The parent compound BA shows the widest E_{HL} of 3.9 eV and the largest ΔE_{ST} of 0.67 eV, indicating strong orbital overlap and limited charge-transfer character, which suppresses TADF. In contrast, TBA–Ac, BBAC–Ac, and BBAPC–Ac exhibit narrower E_{HL} and significantly reduced ΔE_{ST} values, reflecting enhanced charge-transfer properties and spatial separation between HOMO and LUMO. This thereby facilitates efficient reverse intersystem crossing. Overall, the progressive lowering of both E_{HL} and ΔE_{ST} across the series confirms that donor–acceptor tuning effectively modulates electronic properties and promotes TADF activity in these boron-based emitters.

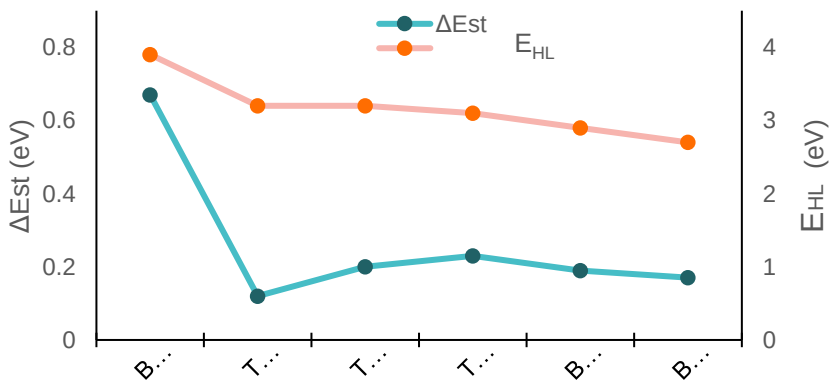

Figure 3.4. Correlation between E_{HL} and ΔE_{ST}.

The calculated optical absorption spectra provide further insight into the excited-state characteristics of the materials. (Figure 3.5) This reveals strong absorption bands in the UV-Visible region corresponding to the transitions, consistent with the charge-transfer nature. The simulated optical absorption spectra of the studied boron-based compounds provide clear evidence of how donor substitution modulates their electronic structures. The parent molecule, BA, exhibits a sharp absorption peak around 250 nm in the ultraviolet region, corresponding to a localized π–π* transition within its rigid framework. This strong, narrow band indicate limited intramolecular charge transfer and strong orbital localization, consistent with the absence of donor groups and minimum charge transfer properties. With the introduction of donor substituents such as acridine and carbazole, the absorption peaks progressively redshift toward longer wavelengths. This shift signifies enhanced donor–acceptor coupling and increased CT character. Among the derivatives, *TBA-Ac, TBA-3Cz, BBAC-Ac* and *BBAPC-Ac* show redshift into the near visible region. *TB-P3Cz* shows a prominent shift of peak to the visible region around 450 nm. *BBAPC–Ac* in particular, displays the most intense absorption band, likely attributed to its phenyl-carbazole donors, which strengthen CT transitions from donor to the boron-based acceptor. The redshift of absorption spectrum of *BA* to that of *BBAPC-Ac* thus demonstrates systematic tuning of optical properties through donor engineering. These optical features are consistent with the HOMO–LUMO analysis and suggest that the derivatives possess favourable electronic configurations for efficient reverse intersystem crossing, making them promising candidates for TADF-based optoelectronic applications.

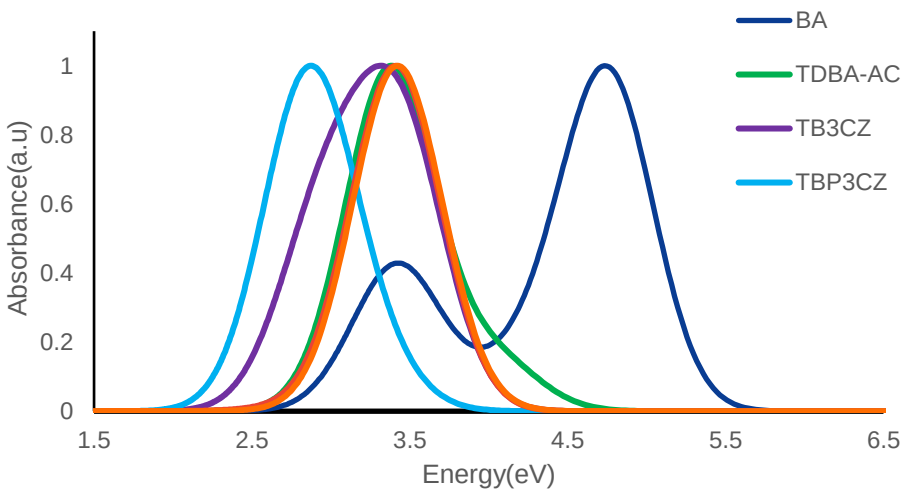

Figure 3.5. Normalized optical absorption spectra of the investigated materials

Among the derivatives, TB3CZ and BBAPC-AC display closely aligned absorption maxima near 3.4 eV, suggesting similar electronic coupling between donor and acceptor moieties. The redshift observed in these donor-substituted compounds compared to BA confirms that donor incorporation extends π-conjugation and stabilizes the excited state. The broadness of the peaks also indicates increased charge-transfer contribution, characteristic of efficient

TADF emitters. Overall, the spectral shifts demonstrate that tuning donor strength and substituent position effectively modulates the optical and electronic properties of boron-based TADF materials.

The k_{RISC} governs the efficiency of the triplet-to-singlet conversion process that enables TADF. To predict the k_{RISC}, the calculated values were integrated into the simplified Fermi's golden rule equation assuming an ambient temperature of 298.15 K for comparison. The calculated *SOCME* values between the S_1 and T_1 states, $|\langle S_1|\hat{H}_{SOC}|T_1\rangle|$, reorganization energies (λ_{RISC}) of RISC processes calculated by the four-point method and the resulting predicted rates are summarized in Table 3.1. The kinetic data clearly differentiates the derivative compounds. The parent compound *BA* shows a negligible rate, which can be directly linked to its large ΔE_{ST} of 0.68 eV), high λ_{RISC} of 0.58 eV, and very weak *SOCME* of 0.03 cm^{-1}. confirming its unsuitability as a TADF emitter. The large singlet–triplet separation and minimal spin–orbit interaction essentially prevents the triplet excitons from being converted to singlets. In contrast, the boron-based derivatives exhibit values in the range of 10^3 to 10^6, which is indicative of highly efficient TADF materials.

The magnitude of k_{RISC} is determined primarily by three key parameters: the ΔE_{ST}, the λ_{RISC} and the $|\langle S_1|\hat{H}_{SOC}|T_1\rangle|$. A small ΔE_{ST} reduces the thermal activation barrier between the S_1 and T_1 states, a small λ_{RISC} minimizes geometric and electronic rearrangements during the spin-flip transition, and a large *SOCME* enhances the probability of spin–orbit coupling between the states. Thus, an ideal TADF emitter combines these three features to achieve a fast RISC process.

Table 3.1. Summary of the key TADF parameters of the investigated materials and predicted k_{RISC} values

Material	S_1 **(eV)**	T_1 **(eV)**	ΔE_{ST} **(eV)**	S_1/T_1 **(Previous work)**	λ_{RISC} **(eV)**	$\langle S_1\|\hat{H}_{SOC}\|T_1\rangle$ **(cm^{-1})**	k_{RISC} **(s^{-1})**
BA	3.41	2.74	0.67	3.12/2.97 (Hiroki Hirai, 2015,)	0.58	0.03	9.67×10^{-7}
TBA-Ac	2.70	2.58	0.12	3.11/3.05 (Shantaram S. Kothavale, 2020)	0.41	1.54	1.26×10^{6}
TBA-3Cz	2.95	2.75	0.20	2.91/2.84 (Hyung Jong Kim, 2020)	0.46	0.18	1.54×10^{3}
TBA-P3Cz	2.85	2.61	0.23	2.81/2.70 (Hyung Jong Kim, 2020)	0.50	0.725	5.66×10^{3}
BBAC-Ac	2.57	2.37	0.19		0.41	1.14	8.55×10^{4}
BBAPC-Ac	2.35	2.17	0.17		0.31	1.19	4.04×10^{5}

TBA-3Cz and TBA-P3Cz show moderate RISC rates. Their ΔE_{ST} values and higher λ_{RISC} indicate greater structural reorganization during excitation, while the relatively weaker SOCME limits the spin–orbit interaction strength. These combined effects slow down the upconversion process compared to the best-performing emitters.

BBAPC-Ac and BBAC-Ac also display efficient RISC processes due to the combination of small ΔE_{ST}, relatively low λ_{RISC} values and strong *SOCME*. Their extended π-conjugation and rigid donor–acceptor frameworks help maintain similar geometries between the S_1 and T_1 states, enhancing spin–orbit coupling. These characteristics enable a balance between electronic coupling and molecular rigidity, which is crucial for achieving efficient triplet harvesting.

In contrast, TBA-Ac exhibits the highest k_{RISC} value of 1.26×10^6 s^{-1}, reflecting an exceptionally efficient RISC process. This high rate can be attributed to its small ΔE_{ST}, low λ_{RISC}, and strong *SOCME*. The strong spin–orbit interaction promotes significant mixing of singlet and triplet wavefunctions, while the minimized energy gap allows thermal population of the singlet state even at room temperature, confirming TBA-Ac as a highly promising TADF emitter.

Overall, the trend in RISC efficiency follows the order

$$\text{TBA-Ac} > \text{BBAPC-Ac} > \text{BBAC-Ac} > \text{TBA-P3Cz} > \text{TBA-3Cz} \gg \text{BA}$$

This clearly demonstrates that efficient RISC is achieved when ΔE_{ST} and λ_{RISC} are minimized while SOCME is maximized, confirming TBA-Ac as the most promising TADF emitter among the studied compounds.

4. Conclusions

The results demonstrate that molecular modification through donor incorporation significantly influences the excited-state energetics and TADF efficiency. The parent compound BA, with a wide ΔE_{ST} and negligible k_{RISC}, exhibited no thermally activated delayed fluorescence, reflecting inefficient triplet upconversion. In contrast, the derivatives exhibited substantially smaller ΔE_{ST} values, enabling more favourable reverse intersystem crossing. Among the investigated systems, TBA–Ac displayed the smallest ΔE_{ST} and highest SOCME, yielding the fastest k_{RISC}, indicating efficient singlet-triplet conversion and suggesting its superior potential as a TADF emitter. The reorganization energy was found to range between 0.30–0.57 eV, suggesting moderate structural relaxation between singlet and triplet manifolds, which complements favourable RISC dynamics. Our findings highlight how strategic donor substitution and steric modulation around the boron–oxygen core effectively tailor photophysical properties for efficient thermally activated delayed fluorescence.

This study establishes a clear quantitative correlation between molecular structure and TADF performance in boron-based donor-acceptor systems. The systematic decrease in ΔE_{ST} coupled with enhanced SOC and RISC rates confirms that strategic donor engineering

enables efficient triplet utilization in purely organic frameworks. The insights gained not only advance the understanding of boron-centered TADF emitters but also provide a theoretical foundation for the rational design of sustainable, high-efficiency, metal-free OLED materials.

Acknowledgement

The authors are grateful to the Research Centre of Shahjalal University of Science and Technology, Sylhet, Bangladesh for financial support.

References

[1] A. Endo, M. O. (2009). Thermally activated delayed fluorescence from Sn 4+–porphyrin complexes and their application to organic light-emitting diodes— A novel mechanism for electroluminescence, *Advanced Materials*, 4802–4806. doi:https://doi.org/10.1002/adma.200900983

[2] Adachi, C. (2014). Third-generation organic electroluminescence materials, *Japanese Journal of Applied Physics, 53*(6). doi:10.7567/JJAP.53.060101

[3] Baldo, M. A., O'Brien, D. F., You, Y., Shoustikov, A., Sibley, S., Thompson, M. E., & Forrest, S. R. (1998). Highly efficient phosphorescent emission from organic electroluminescent devices, *Nature, 395*(6698), 151-154. doi:https://doi.org/10.1038/25954

[4] Bässler, A. K. (n.d.). *Electronic Processes in Organic*, Wiley-VCH.

[5] Dae Hyun Ahn, S. W. (2019). Highly efficient blue thermally activated delayed fluorescence emitters based on symmetrical and rigid oxygen-bridged boron acceptors, *Nature Photonics, 13*. doi:https://doi.org/10.1038/s41566-019-0415-5

[6] Endo, A., Sato, K., Yoshimura, K., Kawada, A., Miyazaki, H., & Adachi, C. (2011). Efficient up-conversion of triplet excitons into a singlet state and its application for organic light emitting diodes, *Applied Physics Letters 98*. doi:https://doi.org/10.1063/1.3558906

[7] Frank Neese. (2012). The ORCA program system, *WIRES Computational Molecular Science*. doi:https://doi.org/10.1002/wcms.81

[8] Gloria Hong, X. G. (2021). A brief history of OLEDs—Emitter development and industry milestones. *Advanced Materials, 33*(9). doi: https://doi.org/10.1002/adma.202005630

[9] Gross, E. R. (1984). Density-functional theory for time-dependent systems, *Physics Review Letters 52*, 997. doi:https://doi.org/10.1103/

[10] H. Yersin, A. F. (2011). The triplet state of organo-transition metal compounds. Triplet harvesting and singlet harvesting for efficient OLEDs, *Coordination Chemistry Reviews*, 55: 2622–2652. doi:https://doi.org/10.1016/j.ccr.2011.01.042

[11] H. Chermette. (1998). Density functional theory: A powerful tool for theoretical studies in co-ordination chemistry, *Coordination Chemistry Reviews*. doi:https://doi.org/10.1016/S0010-8545(98)00179-9

[12] Hiroki Hirai, K. N. (2015,). One-step borylation of 1,3-diaryloxybenzenes towards efficient materials for organic light-emitting diodes, *Angewandte Chemie*, 127,

13785 –13789.
[13] Hiroki Uoyama, K. G. (2012). Highly efficient organic light-emitting diodes from delayed fluorescence, *Nature, 492*, 234–238. doi:https://doi.org/10.1038/nature11687
[14] Hyung Jong Kim, M. G. (2020). Color-tunable boron-based emitters exhibiting aggregation-induced emission and thermally activated delayed fluorescence for efficient solution-processable nondoped deep-blue to sky-blue OLEDs, *Advanced Optical Materials* 8(14). doi: https://doi.org/10.1002/adom.201902175
[15] J. H. Burroughes, D. D. (1990). Light-emitting diodes based on conjugated polymers, *Nature, 347*, 539–541. doi:https://doi.org/10.1038/347539a0
[16] M. J. Frisch, G. W. (2016). *Gaussian 16*, Wallingford CT: Gaussian, Inc.
[17] Reineke, S. (2014). Phosphorescence meets its match, *Nature Photonics*, *8*, 269–270. doi:https://doi.org/10.1038/nphoton.2014.78
[18] W.Kohn. (1999). Nobel lecture: Electronic structure of matter-wave functions and density functionals, *Rev.Mod.Phys, 71*, 1253.
[19] Wolfgang, B. (2005). *Introduction to the Physics of Organic Semiconductors.*
[20] Y. Olivier, J.-C. S.-G. (2018). Computational design of thermally activated delayed fluorescence materials: The challenges ahead, *The Journal of Physical Chemistry Letters*, *9(20)*, 6149-6163. doi:10.1021/acs.jpclett.8b02327
[21] Y. Zhang, J. L. (2014). Tenfold increase in the lifetime of blue phosphophosphorescent organic light-emitting diodes, *Nature Communications*, 5:1-7.
[22] Ye Tao, K. Y. (2014). Thermally activated delayed fluorescence materials towards the breakthrough of organoelectronics, *Advanced Materials*, 26:7931–7958.
[23] Youichi Tsuchiya, S. D.-C. (2021). Exact solution of kinetic analysis for thermally activated delayed fluorescence materials, *The Journal of Physical Chemistry A 125, 36*, 8074–8089. doi:https://doi.org/10.1021/acs.jpca.1c04056
[24] Yuyu Pan, W. L. (2014). High yields of singlet excitons in organic electroluminescence through two paths of cold and hot excitons, *Advanced Optical Material, 2*(6), 1-6.